Research Paper

Drug Release from Phase-Changeable Nanodroplets Triggered by Low-Intensity Focused Ultrasound

Yang Cao,[1] Yuli Chen,[1] Tao Yu,[1] Yuan Guo,[1] Fengqiu Liu,[1] Yuanzhi Yao,[1] Pan Li,[1] Dong Wang,[1] Zhigang Wang,[1] Yu Chen[2]✉ and Haitao Ran[1]✉

1. Chongqing Key Laboratory of Ultrasound Molecular Imaging, Institute of ultrasound imaging, Second Affiliated Hospital, Chongqing Medical University, Chongqing, 400010, P. R. China.
2. State Key Lab of High-Performance Ceramics and Superfine Microstructure, Shanghai Institute of Ceramics, Chinese Academy of Sciences, Shanghai, 200050, P. R. China.

✉ Corresponding authors: chenyu@mail.sic.ac.cn and ranhaitao@hospital.cqmu.edu.cn

Abstract

Background: As one of the most effective triggers with high tissue-penetrating capability and non-invasive feature, ultrasound shows great potential for controlling the drug release and enhancing the chemotherapeutic efficacy. In this study, we report, for the first time, construction of a phase-changeable drug-delivery nanosystem with programmable low-intensity focused ultrasound (LIFU) that could trigger drug-release and significantly enhance anticancer drug delivery.

Methods: Liquid-gas phase-changeable perfluorocarbon (perfluoropentane) and an anticancer drug (doxorubicin) were simultaneously encapsulated in two kinds of nanodroplets. By triggering LIFU, the nanodroplets could be converted into microbubbles locally in tumor tissues for acoustic imaging and the loaded anticancer drug (doxorubicin) was released after the microbubble collapse. Based on the acoustic property of shell materials, such as shell stiffness, two types of nanodroplets (lipid-based nanodroplets and PLGA-based nanodroplets) were activated by different acoustic pressure levels. Ultrasound irradiation duration and power of LIFU were tested and selected to monitor and control the drug release from nanodroplets. Various ultrasound energies were introduced to induce the phase transition and microbubble collapse of nanodroplets in vitro (3 W/3 min for lipid nanodroplets; 8 W/3 min for PLGA nanodroplets).

Results: We detected three steps in the drug-releasing profiles exhibiting the programmable patterns. Importantly, the intratumoral accumulation and distribution of the drug with LIFU exposure were significantly enhanced, and tumor proliferation was substantially inhibited. Co-delivery of two drug-loaded nanodroplets could overcome the physical barriers of tumor tissues during chemotherapy.

Conclusion: Our study provides a new strategy for the efficient ultrasound-triggered chemotherapy by nanocarriers with programmable LIFU capable of achieving the on-demand drug release.

Key words: Programmable drug release, Low-intensity focused ultrasound (LIFU), Perfluorocarbon nanodroplets, Ultrasound imaging

Introduction

Ultrasound, as a component of drug-delivery modalities, has many attractive features including simplicity and cost-effectiveness [1-14]. Tumor sonication can be performed non-invasively, and ultrasound wave can be directed toward deeply located tumor sites in precise energy-deposition patterns [15-18]. Microbubbles, known to be the ultrasound contrast agents in the clinic, have been

used to load therapeutic agents for efficient tumor chemotherapy [19-23]. However, the disadvantages of these gas-filled microbubbles hamper their versatile applications in drug delivery. For example, it is difficult to achieve efficient drug concentration in tumor sites because of their limited capacity for loading therapeutic agents, short circulation time, and large micrometer size. To address these problems, phase-change perfluorocarbon (PFC) nanodroplets have been developed [18, 20, 24-27] in which the liquid in the core of nanodroplets can vaporize to gas phase upon activation by ultrasound energy, called acoustic droplet vaporization (ADV) [28-30]. The stability of nanodroplets is increased, and they can accumulate in tumor tissues by passive targeting due to their nano-scaled size. When converged in tumor sites, these nanodroplets convert into microbubbles under targeted ultrasound irradiation. These acoustic microbubbles oscillate and collapse by ultrasound-targeted microbubble destruction (UTMD) effect [22, 31-34]. During this process, the therapeutic agents encapsulated in bubbles are released in tumor cells.

Ultrasound is a form of the longitudinal mechanical wave that can be transmitted in the human body and is widely used in tumor imaging and therapy [30-35]. Different from the diagnostic ultrasound used in the clinic to force bubble elastic compression and expansion, more ultrasound energy is needed to induce conversion of nanodroplets into microbubbles and trigger local drug release [28-32]. However, it is difficult to induce droplet-to-bubble transition and destruction of hard-shelled (e.g. polymer-based) nanodroplets. These hard-shelled bubbles do not show volume expansion at a low acoustic pressure due to the increased damping contribution of the polymer shell, which remains intact until reaching a certain pressure threshold of ultrasound [41, 42].

It has previously been shown that the physical property of shell materials is an important factor that influences the acoustic behavior of microbubbles [15, 36-38]. Upon exposure to low-frequency ultrasound, soft-shelled microbubbles, which are normally lipid-based materials, can generate shock waves, shear forces, and microstream from UTMD effects, promoting extensive intratumoral drug delivery [37-39, 40]. Also, there is an increasing interest in inducing the ADV phenomenon to trigger drug release from nanodroplets employing another type of ultrasound. For example, acoustic energy from focused ultrasound can be delivered to a focal point with millimeter precision by using a focused transducer. High-intensity focused ultrasound (HIFU) has been approved by FDA for the treatment of uterine fibroids [43-45], which is used to induce tumor thermal ablation by heating and to denature proteins during the treatment. During ultrasound imaging, it is important to avoid unwanted thermal damage to obtain a comprehensive tissue imaging. We have developed low-intensity focused ultrasound (LIFU) with limited ultrasound energy [46-48] in which, different from HIFU, mechanical effect is the dominate function which can force bubbles in the acoustic field to oscillate, expand, and collapse. The focused transducer ensures tight focusing of the ultrasonic energy on the target sites precisely.

In this study, we report, for the first time, the construction of phase-changeable drug-delivery nanodroplets with programmable LIFU-triggered drug release for significantly enhanced anticancer drug delivery. Based on the difference of acoustic pressure between soft-shelled and hard-shelled nanosystems, two kinds of nanodroplets (lipid-based nanodroplets, LN; PLGA-based nanodroplets, PN) with encapsulated perfluorocarbon (perfluoropentane, PFP) and anticancer drug doxorubicin (DOX) were fabricated. Since these nanodroplets required different ultrasonic pressures for phase transformation and drug release, two parameters of LIFU were chosen to activate DOX release from the LN and PN nanodroplets at pre-determined time points. By accurate acoustic-energy deposition and co-administrating multiple nanodroplets, a programmable drug-releasing profile was achieved which could efficiently increase therapeutic effectiveness and decrease the course of chemotherapeutic treatment, as demonstrated by both *in vitro* and *in vivo* studies. Thus, ultrasound was used not only to monitor tumors but also as a useful and powerful tool for modulating the programmable drug release for efficient tumor chemotherapy.

Experimental section

Materials and reagents

Poly(lactide-co-glycolide)-co-poly (ethylene glycol) (mPEG5000-PLGA, MW: 15 kDa) was purchased from Jinan Daigang Bio-Tech. Inc., Jinan, P. R. China. 1,2dipalmitoyl-sn-glycerol-3-phosphatidylcholine (DPPC), 1,2-dipalmitoyl-sn-glycerol-3-phospho-(1-rac-glycerol) (DPPG), and dipalmitoylphosphatidyl-ethanolamine-polyethyleneglycol-2000 (DPPE-PEG 2000) were purchased from Avanti Polar Lipids, Inc. (Alabaster, AL). Perfluoropentane (PFP) and doxorubicin hydrochloride (DOX) were obtained from Apollo Scientific Ltd (Cheshire, UK) and J&K China Chemical Ltd (Beijing, P. R. China), respectively. All other reagents were of analytical grade.

Human breast cancer cell line MDA-MB-231 was supplied by the Institute of Ultrasound Imaging of Chongqing Medical University. The cells were maintained in high glucose Dulbecco's Modified Eagle Medium (DMEM) supplemented with 10% fetal bovine serum (FBS) and 1% penicillin/streptomycin. Four-week-old BALB/c female nude mice were supplied by the Laboratory Animal Center in Chongqing Medical University and fed in accordance with the guidelines of the local animal care committee of Chongqing Medical University. All animal experimental procedures were approved by the Animal Ethics Committee of Chongqing Medical University.

Preparation and characterization of drug-loaded nanodroplets

Drug-loaded lipid nanoemulsions were prepared using a simple thin-film hydration-sonication method. Typically, a mixture of DPPC, DPPG, DPPE, and cholesterol with a mass ratio of 5:1.5:2:1.5 was dissolved in chloroform (5 mL) and transferred to a round bottom flask to form a thin film by rotary vacuum evaporation at 55 °C. The phospholipid film was hydrated with 2 ml of DOX solution (0.5 mg/ml, w/v). The suspension was sonicated in an ice bath using a microtip probe of the sonicator (VCX-130, Sonics & Material Inc., Newtown, CT, USA) at a power output of 103 W for two minutes. Then, liquid PFP (200 µL) was added and sonicated at 20s pulse duty cycle for 2 min. The mixtures were centrifuged at 10,000 rpm for 5 minutes and then washed three times to remove the un-encapsulated drug.

The double emulsion method was adopted to fabricate PLGA-based nanoemulsions. For this, mPEG-PLGA (50 mg) was dissolved in dichloromethane (5 mL). PFP (200 µL) was added and sonicated at 20s pulse duty cycle for 2 min in an ice bath. Then, the DOX solution and poly (vinyl alcohol) (PVA, MW=25 000 kDa, 20 mL, 4% w/v) solution were added into suspension and homogenized (FJ300-SH, P. R. China) in ice bath for 2 min. After further stirring, the mixture was centrifuged at 10,000 rpm for 5 minutes and then washed three times to remove the un-loaded drug.

Dynamic light scattering (DLS) methods were used to measure particle diameters and size distribution at 20°C by Zetasizer Nano ZS 90 instrument (Malvern Instruments Ltd., Malvern, UK). The values were determined by the mean value of three independent measurements. Nanodroplets were incubated with 10% fetal bovine serum at different times to investigate the size stability. For transmission electron microscope (TEM, FEI Tecnai 10, Philips Electron Optics, Holland) observation, nanodroplet dispersions were deposited on formvar film-coated copper grids after staining by phosphomolybdic acid hydrate.

In vitro liquid-gas phase transition and responsive drug release activated by LIFU

The nanodroplets were added into the pre-formed wells of an agarose gel phantom (3% agarose). Then, the LIFU transducer (1 MHz, acoustic intensity: 1.2 W/cm², duty cycle: 50%, Chongqing Medical University, P. R. China) was placed perpendicular to the surface of the gel wells. The nanodroplets were exposed to the LIFU irradiation with the power of 1-8 W and duration of 1-5 min. Harmonic ultrasound-imaging signals of the post-formed microbubbles from nanodroplets were observed in real-time by MyLab 90 ultrasound diagnostic system (Esaote, Italy). The average ultrasound intensity was determined by DFY software (Chongqing Medical University, P. R. China).

For measuring the drug-releasing patterns, the drug-loaded droplets were collected and incubated in a conical flask with 20 mL of pre-warmed PBS (100-120 rpm/min) at 37°C. As for LN-PN group, LN and PN in PBS were mixed with DOX at a molecular ratio of 1:1. LIFU was applied for the active drug release. At pre-determined time intervals (8 h and 18 h), a 2 mL release medium was taken out for measurement. The same amount of fresh buffer was then added to maintain the sink condition. The DOX concentrations were determined at 483 nm by UV-vis spectrometry (Lambda 900, PerkinElmer, USA). The encapsulation efficiency (EE) was defined as the ratio of actually loaded and original amount of drug. The drug-loading content was calculated as the ratio of actually loaded drug and the total drug/carrier amount. The accumulated release percentage of drug was determined as

$$Q(\%) = \frac{C_n \cdot V + V_i \sum_{i=0}^{n-i} C_i}{m_{drug}} \times 100\%$$

Here, Q (%) was the accumulated concentration of released drugs. V (mL) was the total volume of samples. C_n (mg/mL) and V_i (mL) were the concentration and volume of samples taken at n and i time point. m_{drug} (mg) was the drug mass in particles. The number of times of the release media replacements was numbered as n.

Cytotoxicity and cell apoptosis assay (annexin V/propidium iodide protocol)

Human breast cancer cells MDA-MB-231 were

routinely cultured in high glucose DMEM with 10% fetal bovine serum (FBS) and 1% penicillin/streptomycin at 37°C, 5%CO$_2$. MDA-MB-231 cells were seeded in 96-well plates at 2×10^4 cells per well and incubated at 37°C, 5%CO$_2$ for 24 h. The cells were exposed to the fresh culture medium containing the respective samples. The groups of free DOX and drug-loaded nanodroplets had the same concentration of DOX (30 μg/mL). The culture medium was replaced with 20 μL MTT solutions (5 mg/mL, w/v) and 180 μL serum-free medium at the end of the incubation time (24 h, 48 h, and 72 h). The plates were incubated for another 4 h at 37°C, 5%CO$_2$. Washing with PBS was followed by the addition of 150 μL DMSO to dissolve the formazan crystals and gentle shaking for 10-20 min to achieve complete dissolution. The absorbance was recorded at 490 nm using the microplate spectrophotometer system. The viability percentage was expressed as absorbance in the presence of drug-loaded nanodroplets as a percentage of that of the vehicle control.

Two-color flow cytometric analysis was used to investigate the cellular apoptosis after drug-loaded nanodroplets were activated by LIFU. The substances were collected and added to the plates. MDA-MB-231 cells were collected at the end of incubation. Cells were washed with PBS and stained with reagents from Apoptosis Assay Kit (Bestbio Co. Ltd, P. R. China) following the manufacturer's instruction and analyzed using a flow cytometer (FACSVantage SE, BD Biosciences, US).

Cellular uptake of nanodroplets

MDA-MB-231 cells (2×10^4) were seeded into confocal culture dishes in DMEM supplemented with 10% FBS and 1% penicillin/streptomycin for 24 h. After the medium was substituted with serum-free medium with nanodroplets samples, the cells were incubated at 37 °C, 5% CO$_2$ for 4 h. The cells were washed with PBS twice and fixed with 4% paraformaldehyde. Subsequently, cells were stained fluorescently by DiO and DAPI after washing with PBS. Intracellular uptake of nanodroplets was investigated under a confocal laser scanning microscope (Olympus FV1200, Tokyo, Japan) and inverted fluorescence microscope (Olympus IX53, Tokyo, Japan).

In vivo tumor imaging

Four-week-old BALB/c female nu/nu mice were supplied by the Laboratory Animal Center in Chongqing Medical University and maintained in accordance with the guidelines of the local animal care committee. All animal experimental procedures were approved by the Animal Ethics Committee of Chongqing Medical University. MDA-MB231 cells were grown in nu/nu mice by subcutaneous inoculation of 2×10^5 cells. When the tumors grew to a volume of approximately 80-100 mm^3, 200 μL of the mixture (an equivalent DOX concentration of 1.0 mg/mL) in 0.9% saline solution was injected intravenously into the tail vein of the mouse.

The ultrasound transducer (1 MHz, acoustic intensity:1.2 W/cm^2, duty cycle:50%, Chongqing Medical University, P. R. China) was fixed above the tumor in contact with a gel interface coupled with an extra 1.5 cm thick gel bag. Two LIFU parameters (3 W, 3 min; 8 W, 3min) were chosen to activate the phase transition of nanodroplets at 3 min and 5 min. Fundamental and harmonic imaging signals of bubbles were observed in real-time by MyLab 90 ultrasound diagnostic system (Esaote, Italy). Average ultrasound intensity values were measured by DFY software (Chongqing Medical University, P. R. China).

In vivo distribution of nanodroplets and DOX

For pharmacokinetic experiments, BALB/c nude mice bearing tumors were injected intravenously with nanodroplets in 0.9% saline solution. 15 μL blood was collected by enucleation of eyeballs at various times (0 min, 5 min, 10 min, 0.5 h, 1 h, 2 h, 4 h, and 24 h) after injection. The blood samples were dispersed into physiological saline (1 mL) containing 10 mmol/mL EDTA as an anticoagulant. The blood retention time of nanodroplets was calculated by a single-component pharmacokinetic model.

For ultrasound treatment groups, tumors were sonicated with LIFU. The ultrasound transducer was fixed above the tumor in contact with a gel interface coupled with an extra 1.5 cm thick gel bag. PN-LN LIFU1 (LIFU radiation parameter: 5 W, 3min) and PN-LN LIFU2 (LIFU radiation parameter: 1st: 5 W, 3 min, 2nd: 8 W, 3 min) were carried out. The *in vivo* distribution of DiR-stained nanodroplets was imaged using an IVIS spectrum imaging system (PerkinElmer, Waltham, MA, US).

The accumulated concentrations of DOX in various organs were investigated. After treatments, mice were sacrificed and the main organs (tumor, kidney, spleen, lung, liver, heart) were excised, weighed, and extracted with two volumes of acetonitrile/methanol (1:1, v/v). The suspensions were centrifuged and filtered through a 0.22 μm pore cellulose acetate membrane. Drug concentrations in solutions were determined using a UV spectrophotometer.

In vivo anti-tumor effect

BALB/c nude mice xenografted with MDA-

MB-231 cells were randomly divided into groups. The control group was treated with saline. The ultrasound groups were sonicated by LIFU as described above. Samples (0.2 mL) were administrated via the tail vein. The tumor volume was monitored by caliper measurement every two days and calculated by the following equation: Volume=$0.5 \times L \times W^2$. L and W are the length and the width of the tumors, respectively. The survival was determined based on death date from the date of the first injection of each group. Mice with tumor volumes over 1.5 cm diameter had to be sacrificed according to institute guidelines.

Histology and immunohistochemistry experiments were carried out. The tumors of different groups were collected and subjected to Hematoxylin/Eosin (H&E) staining. To assess tumor cell proliferation, immune histochemical staining with antibodies against proliferating cell nuclear antigen (PCNA) was performed. The microvessel density (MVD) of tumor tissues was assessed by CD31 immuno-histochemical staining. The tumor sections were stained with CD31 primary antibody. The sections were imaged by a light microscope. Apoptosis in situ was detected by TdT-dependent dUTP-biotin nick end labeling (TUNEL) assay using apoptosis detection kit.

Statistical analysis

All experiments were performed in triplicates, and the results are presented as mean ± standard deviations. Statistical analyses of the experimental data from different groups were performed by applying one-way ANOVA. A value of $p < 0.05$ was considered significant, and $p < 0.01$ was considered highly significant.

Results and Discussion

Fabrication and characterization of nanoemulsions

Two types of nanodroplets, including PLGA and lipid nanodroplets (Fig. 1A1, 1A2, 1B1 and 1B2), were fabricated in this study. Based on the dynamic light scattering (DLS) measurement (Fig. 1A3 and 1B3), the average diameters of PLGA nanodroplets (PN) and lipid nanodroplets (LN) were around 357.1 ± 15 nm and 409.4 ± 24.7 nm, respectively. It has been reported that the particle size of nanocarriers between 380 nm and 780 nm can be passively targeted to tumor sites through large inter-endothelial gaps [49-52]. The zeta potential of PN was -21.6 ± 3.5 mV and -42.2 ± 6.5 mV for LN. The negative zeta potential may facilitate the nanodroplets to repel each other and prevent aggregation *in vivo*. Upon incubation with serum, these nanodroplets were stable, and the diameters

kept steady in the first four hours while increasing slightly thereafter (Fig.S1, Supporting Information). The results indicated the stability of nanodroplets in serum.

In vitro phase transition and drug release activated by LIFU

We selected adequate ultrasound irradiation power and duration of LIFU to induce phase-change of perfluorocarbon incorporated in nanoemulsions. The harmonic images were taken when nanodroplets were converted into microbubbles by LIFU irradiation. DFY software programmed by our lab was applied to evaluate the value of average ultrasound-signal intensity. Using an LIFU transducer, the ultrasound energy was focused onto the nanodroplets. As shown in Fig. 2A, LN samples had the highest average ultrasound-signal values at the ultrasound parameters of 3 W/3 min, suggesting that a large number of lipid nanodroplets were converted to microbubbles. Since the instability of microbubbles was higher than that of nanodroplets, microbubbles were easier to collapse. With the increase in irradiation power and duration, some lipid microbubbles were destructed and collapsed decreasing the intensities of harmonic ultrasound images. Therefore, the ultrasound-irradiation parameter of 3 W/3 min was selected to activate the phase transition of lipid nanodroplets and release of the loaded drug after bubble collapse. In groups of PN, the ultrasound energy of LIFU (3 W, 3 min) was not high enough to induce conversion of a large number of nanodroplets into microbubbles which may be due to the stiffness of PLGA shell. The value of average ultrasound intensity of harmonic image elevated with the increase of ultrasound energy. The highest average ultrasound-intensity values occurred at the LIFU parameter of 8 W/3 min, which could be employed to induce the phase transition of PLGA nanodroplets. These data showed that LN and PN, due to the specific characteristics of their shell materials such as the shell stiffness difference, had two different ultrasound parameters for inducing PFP phase change and microbubble oscillation. The different ultrasound parameters between LN and PN offered an opportunity to induce sequential conversion of PFP-encapsulated nanodroplets to bubbles. Following conversion of nanodroplets into bubbles, tumor-imaging signals could be collected, and the drug could be released after the collapse of microbubbles.

The therapeutic anticancer agent (DOX) and phase-changeable PFP were concurrently encapsulated into two nanodroplets. Two ultrasound parameters could be adopted independently to induce

sequential liquid-gas phase transition for PN and LN leading to programmable drug release triggered by LIFU. DOX encapsulation efficiency of PN and LN was $84.3 \pm 7.2\%$ and $89.7 \pm 8.8\%$, respectively. To investigate drug-releasing behavior under LIFU irradiation, three groups were formed, namely, PN-LN (control sample, without LIFU radiation), PN-LN LIFU1 (LIFU radiation parameter: 5 W, 3 min), PN-LN LIFU2 (LIFU radiation parameter: 1st: 5 W, 3 min, 2nd: 8 W, 3 min). As displayed in Fig. 3A, DOX was continuously released from the nanodroplets without LIFU radiation but burst release of the drug was observed in the nanodroplets after LIFU exposure. For PN-LN LIFU1, the cumulative drug-releasing percentage increased by 20% at 8 h with subsequent slow drug release from the nanodroplets. Two burst drug-releasing curves were observed in PN-LN LIFU2 groups. About 30% of the drug was released in the initial 8 h. The percentage of cumulative drug release increased up to 50% at the first LIFU triggering. The second LIFU radiation triggered 20% more drug release at the 18 h time point.

We also investigated the drug release profiles of mono nanodroplets (Fig.S2-S3, Supporting Information). The results showed that DOX was released from the LN at 8 h by LIFU1. Liquid PFP encapsulated in LN nanodroplets could change to the gas phase in the ultrasound field. Subsequently, ultrasound microbubbles were formed and exploded resulting in drug release from the nanosystems. In LN LIFU2, the drug release was increased slightly when a second LIFU was employed. The reason for this may be that ultrasound could activate the diffusion of water and drug molecules leading to a greater drug release from the nanoparticles. Unlike the previous drug release profiles from UTMD effect under the LIFU1 at 8 h, this function was not high enough to trigger another burst release. Furthermore, ultrasound could disrupt the condense polymer structure to release the entrapped drugs, which are otherwise difficult to diffuse out of the carriers freely.

As for PN nanodroplets, a significant burst drug release was observed when LIFU2 was utilized. Because of the difference in the rigidity of shell materials, PN and LN required different ultrasound energies to induce droplet-to-bubble transition. Only LIFU2 condition could lead to PN phase transition. Compared with the control group (PN), more drug was released following 8 h LIFU exposure in the PN LIFU1 group due to two factors. The first one is the movement of release medium and drug molecules similar to that of LN. The other one is that a small fraction of PN could change to microbubbles under LIFU1 because of the heterogeneity of PLGA nanodroplets. Although small, ultrasound-signal values of PN could be observed at the ultrasound parameters of 3 W/3 min suggesting some PLGA nanodroplets were changed to microbubbles under LIFU1 irradiation (Figure 2). Size diameter is known as one of the important parameters to induce the phase transition of PFC encapsulated nanodroplets. The larger nanodroplets had lower transition parameters than that of smaller ones. Therefore, DOX was also released from the PN under LIFU1 exposure.

External ultrasound radiation is necessary for the ultrasound-mediated drug delivery. Drug-loaded microbubbles can be monitored by ultrasound imaging. Once they are detected in the target tissues by diagnostic ultrasound, UTMD can be induced to release therapeutic agents. Liquid PFP encapsulated in nanodroplets change to gas phase under the ultrasound field. Subsequently, ultrasound microbubbles are formed and exploded resulting in drug release from the nanosystems. In this study, because of the different rigidity of shell materials, PN and LN required different ultrasound energies to induce droplet-to-bubble transition. Therefore, two LIFU parameters were employed. At the LIFU1 treatment, the phase transition of LN occurred. Lipid microbubbles were crushed, and the loaded drugs were released leading to the burst drug-releasing profiles after 8 h. Comparatively, only a small fraction of PN was changed to microbubbles under LIFU1. Subsequently, the second burst release of drug originated mainly from the second LIFU exposure at 20 h. In the control group, no obvious burst drug-releasing profiles were observed because no external stimulus was used and liquid perfluorocarbon kept steady and did not change to the gas phase. Drugs released slowly from the nanocarriers when incubated at 37°C within 72 h. Although the mechanism of ultrasound-triggered drug release is not fully understood, a possible mechanism may involve the phase-transition behavior under the ultrasound radiation [15]. It has been reported that the decrease of the initial thickness of the bubble shell may significantly increase the surface area per copolymer molecule, which is beneficial for encapsulated drugs transferring from bubble to the neighboring cells [15]. Furthermore, gaps between the shell polymer molecules became larger after the expansion of bubbles resulting from the ultrasound radiation which may facilitate the escape of drug molecules from bubbles. Since lipid materials presented better elasticity than PLGA, LN bubbles could easily expand under the same LIFU parameters.
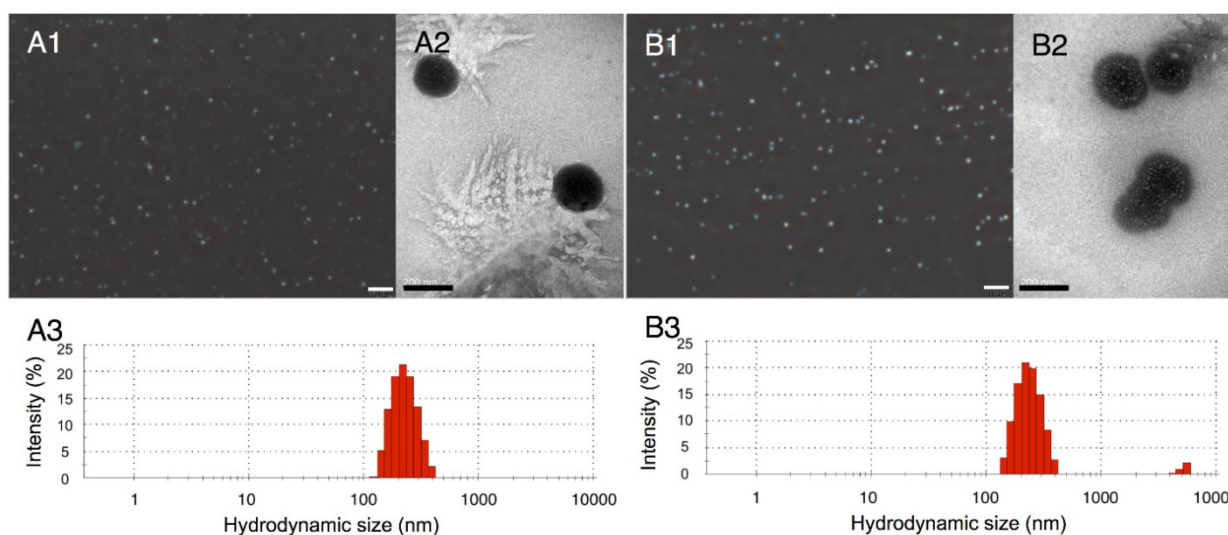
Figure 1. Optical images of PLGA nanodroplets (A1) and lipid nanodroplets (B1) (presented as mean ± standard deviations (scale bar=10 µm); TEM image of PLGA nanodroplets (A2) and lipid nanodroplets (B2) (scale bar=200 nm); Size distribution of PLGA nanodroplets (A3) and lipid nanodroplets (B3).
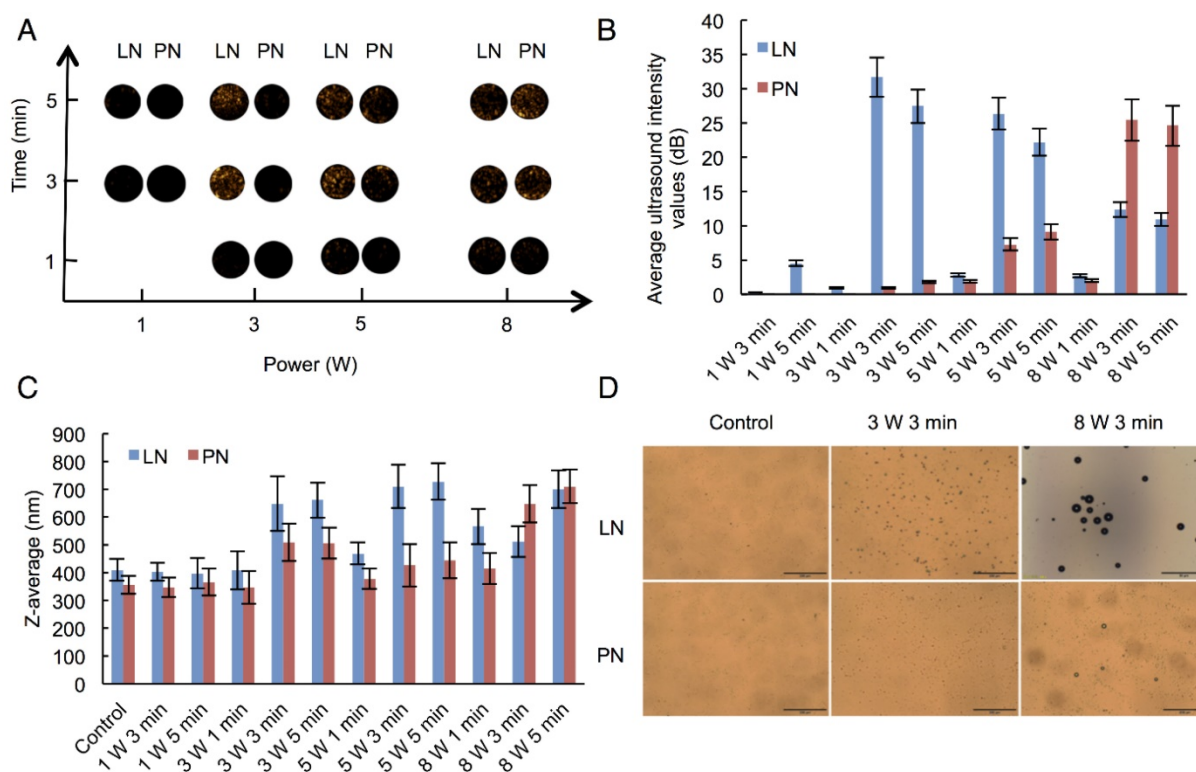

Figure 2. Harmonic images (A), average ultrasound intensity values (B), average diameters (C) and optical images (D) of two types of nanodroplets after LIFU irradiation. (The LN 8 W, 3 min group: scale bar=50 µm; The other groups: scale bar=200 µm). Control: nanodroplet without ultrasound exposure.

Cytotoxicity assay and cellular apoptosis induced by LIFU-exposed nanodroplets

To investigate the cytotoxicity and chemotherapeutic efficiency of nanodroplets, various groups of agents were incubated with MDA-MB-231 cells for 72 h. As shown in Fig. 3C, cell viability of groups treated with free DOX or drug-loaded LN-PN decreased with incubation time. The free DOX group exhibited mild cytotoxicity compared with that of the control group after incubation for 72 h. On the other hand, the LIFU1-treated group exhibited different cell cytotoxicity (Fig.S4, Supporting Information). There was no significant difference between LIFU1 group and the control group after 24 h and 48 h incubation. After 24-h treatment with LIFU2, MDA-MBA-231 cells exhibited relatively high cell viability of about 90%. The cell viabilities dropped in vitro with increased

incubation time. After incubation for 72 h, cell viabilities were over 80% for both ultrasound treated groups (LIFU1 and LIFU2). MDA-MBA-231 cells exhibited 85.6% cell viability after 24 h incubation with LN-PN. The value decreased to 80% and 62.5% after incubation for 48 h and 72 h, respectively as more drug was released when treated for a longer duration showing a time-dependent therapeutic efficacy. For the group of nude LN-PN, over 90% cells survived after incubation for 72 h, indicating relatively high biocompatibility of lipid and polymeric nanodroplets. In this study, we chose the pulsed ultrasound rather than the continued ultrasound exposure, which may result in cell detachment. Furthermore, the possible effect of the acoustic reflection from the cell culture plates should be avoided in the in vitro experiments. This phenomenon would be minimized by the buffering effect of the in vivo environment.

The intracellular uptake of nanodroplets was further studied by confocal fluorescent microscopy (Fig. 3B). Cell membrane and nucleus were stained by fluorescent agent Dio (green) and DAPI (blue), respectively. After incubation with MDA-MB-231 cells for 24 h, the red fluorescence (nanodroplets) from tumor cells was much stronger in the LN group than that in the PN group. As shown in Fig. 3B, the red fluorescence of PN was observed mostly around the cell membrane. It indicated that DOX from LN was more effectively delivered into cells within 24 h. Comparatively, the intracellular distribution of DOX might require a longer time for the PN group, which was dominated by the interface properties of nanodroplet shells. These temporal and spatial distribution differences between drugs from LN and PN could be used to sequentially kill cancer cells.

Apoptosis of MDA-MB-231 cells after treatment with different agents and conditions were determined by flow cytometric analysis. LIFU was introduced at 12 and 18 h for LN-PN LIFU1 and LN-PN LIFU2 groups. Cells incubated with free DOX showed the highest level of apoptosis among all the groups at the same time point (Fig. 3D). Without ultrasound exposure, apoptosis of the LN-PN group increased steadily with prolonged duration of incubation. However, after LIFU treatment for 12 h, cell apoptosis ratio of LIFU groups (LN-PN LIFU1 and LN-PN LIFU2) was higher than that of LN-PN groups by 6.9% and 5.82%, respectively. Cell apoptosis of LN-PN LIFU2 presented the second highest level after the second LIFU treatment at 18 h hour which was only lower than that of free drug. These results were consistent with the *in vitro* drug-releasing profiles. This indicated that drug-loaded nanocarriers were capable of delivering therapeutic agents into cells efficiently and enhanced the effectiveness of chemotherapy. Also, LIFU was beneficial for triggering drug release in the on-demand fashion.

In vivo ultrasound imaging and biodistribution of nanodroplets with LIFU exposure

The nanodroplet complexes were intravenously injected into BALB/c nude mice xenografted with MDA-MB-231 cancer cells. Fundamental and harmonic ultrasound images of nanodroplets were taken after LIFU irradiation. As shown in Fig. 4A-B, no harmonic ultrasound signals were observed before LIFU exposure. When the first ultrasound (3 W, 3 min) was employed, both fundamental and harmonic ultrasound signals increased in these two groups, indicating that lipid nanodroplets were converted to microbubbles in targets. Subsequently, the second ultrasound irradiation (8 W, 3 min) was carried out in the LIFU2 group. Compared with the LIFU1 group, the second ultrasound radiation induced enhanced acoustic signals suggesting the phase transition of PLGA nanodroplets.

The results of *in vivo* biodistribution of nanodroplets showed accumulation of a large number of nanodroplets in the reticuloendothelial organs, such as liver and spleen (Fig. 4C-D) which were recognized and phagocytosed by macrophages or simply trapped within these organs. Drug-loaded nanocarriers rarely targeted to the tumor sites. Physiology of tumor tissues, such as high interstitial fluid pressure within tumors may prevent nano-carriers from delivering drugs into tumors [53]. LIFU radiation significantly improved the passive targeting efficiency of the nanodroplets which accumulated in the tumor tissue as indicated by high fluorescence. Ultrasound could be used as the physical stimulus to introduce nanodroplets to target the tumor tissues and release their payload only in the lesion sites. Based on this strategy, the drug accumulation and leakage in the normal tissue could be avoided mitigating the harmful systemic side effects.

Fig. 4E shows DOX distribution in different organs after intravenous injection of nanodroplets *in vivo*. Compared to the free DOX group, the accumul-ation of the drug in tumors increased when the drug molecules were encapsulated in the nanodroplets (LN-PN). The ultrasound group displayed a remark-able drug accumulation in tumor tissue as the ultrasound could increase the permeability of tumor vasculature as well as interstitial space locally. Among all four groups, the LN-PN LIFU2 group exhibited the highest DOX accumulation in tumors. When the first ultrasound was introduced, a large number of LN samples transformed to microbubbles and the drug was released after the collapse of the

microbubbles.

It has been previously reported that focused ultrasound in the presence of circulating microbubbles could temporarily open the blood-brain barrier by UTMD effect [54-59]. Under the first ultrasound radiation, the post-formed LN microbubbles might overcome the biological barriers of tumors temporarily. Intratumoral accumulation of PN was enhanced driven by the microjets from lipid bubble destruction. During this process, small pores were generated, and cell membrane permeability was increased permitting the entry of therapeutic agents directly into cancer cells. This process allowed more efficient delivery of PN and DOX from the nanodroplets deep into the tumor tissue after the second ultrasound exposure (Fig. 5). The results indicated the therapeutic drugs could be delivered and released in an on-demand manner by controlling the LIFU. In the case of the injected chemotherapeutic drug, the combination of localized ultrasound exposure of the tumor and microbubbles may provide more opportunities for effective intracellular drug uptake by the tumor cells.

In vivo antitumor efficacy and histological examination

To investigate the chemotherapeutic effect of nanodroplets after LIFU treatment, the tumor volumes were monitored after the intravenous injection of different samples. Fig. 6A displays four tumor-growth curves for control groups, LN-PN, LN-PN LIFU1, and LN-PN LIFU2. The injection time points are indicated by arrows. LIFU radiation (5 W, 3 min) was carried out at the same time point. On the following day, LN-PN LIFU1 and LN-PN LIFU2 groups were further treated by LIFU with different parameters. The tumor volumes of control groups rose sharply and continuously, but the tumor proliferation in both LIFU-treated groups was inhibited. The volumes of tumor tissues remained steady in the first eight days under LIFU treatments because of the release of anti-tumor drug from the LN by LIFU triggering. The tumor growth rate of LN-PN LIFU2 group was slower than that of LN-PN LIFU1 group after the 10th day because more ultrasound energy was utilized to trigger phase change of PN and drug release from the PLGA bubbles. During this time period, the vascular permeability of tumors was increased by the high level of energy from microstreams, shock waves and microjets due to the typical UTMD effect. Thus, the intracellular drug delivery was enhanced and tumor proliferation was efficiently inhibited.
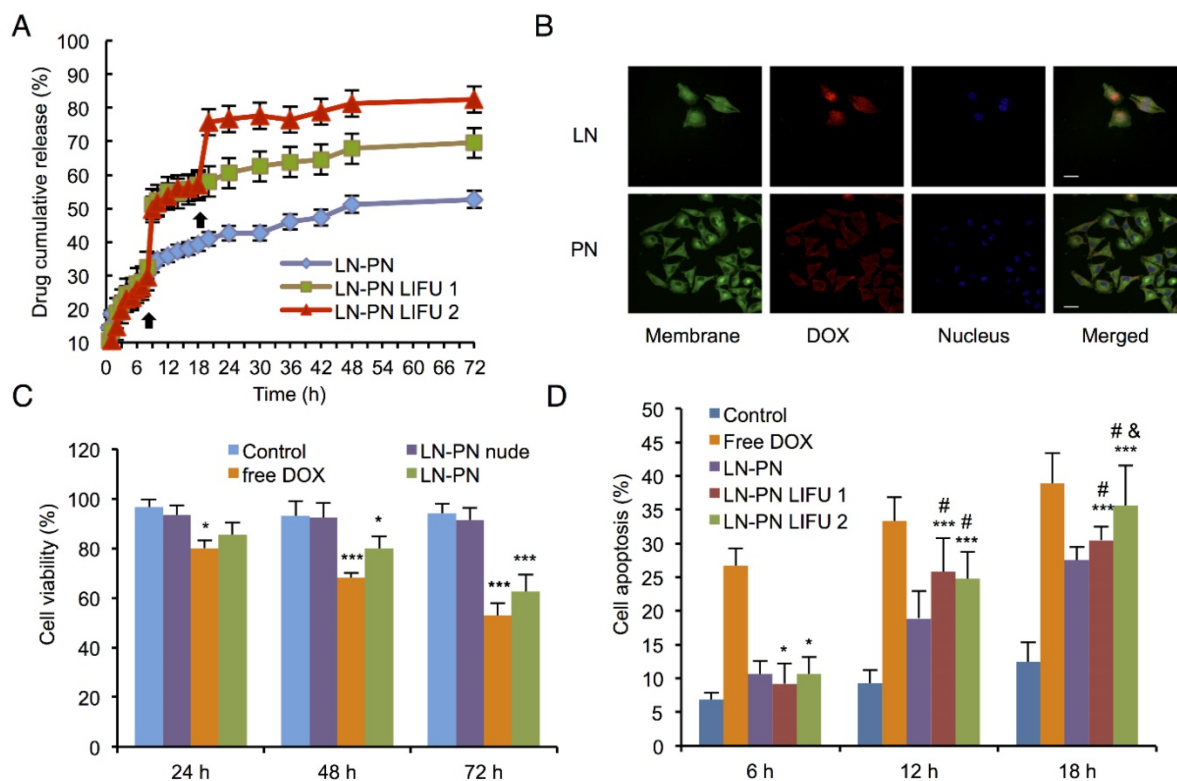

Figure 3. A) Drug-releasing profiles triggered by LIFU under different conditions (black arrow: ultrasound administration); B) Cell uptake observed by confocal fluorescent microscopy (Dio: green, DOX: red, DAPI: blue). Scale bar=10 µm; C) Cell viability of various therapeutic agents (*$p<0.05$ *vs* the control group; ***$p<0.001$ *vs* the control group; #$p<0.05$ *vs* the LN-PN group; $p<0.05$ *vs* the LN-PN LIFU1 group; $n=3$); D) Cell apoptosis in different groups by LIFU treatment.
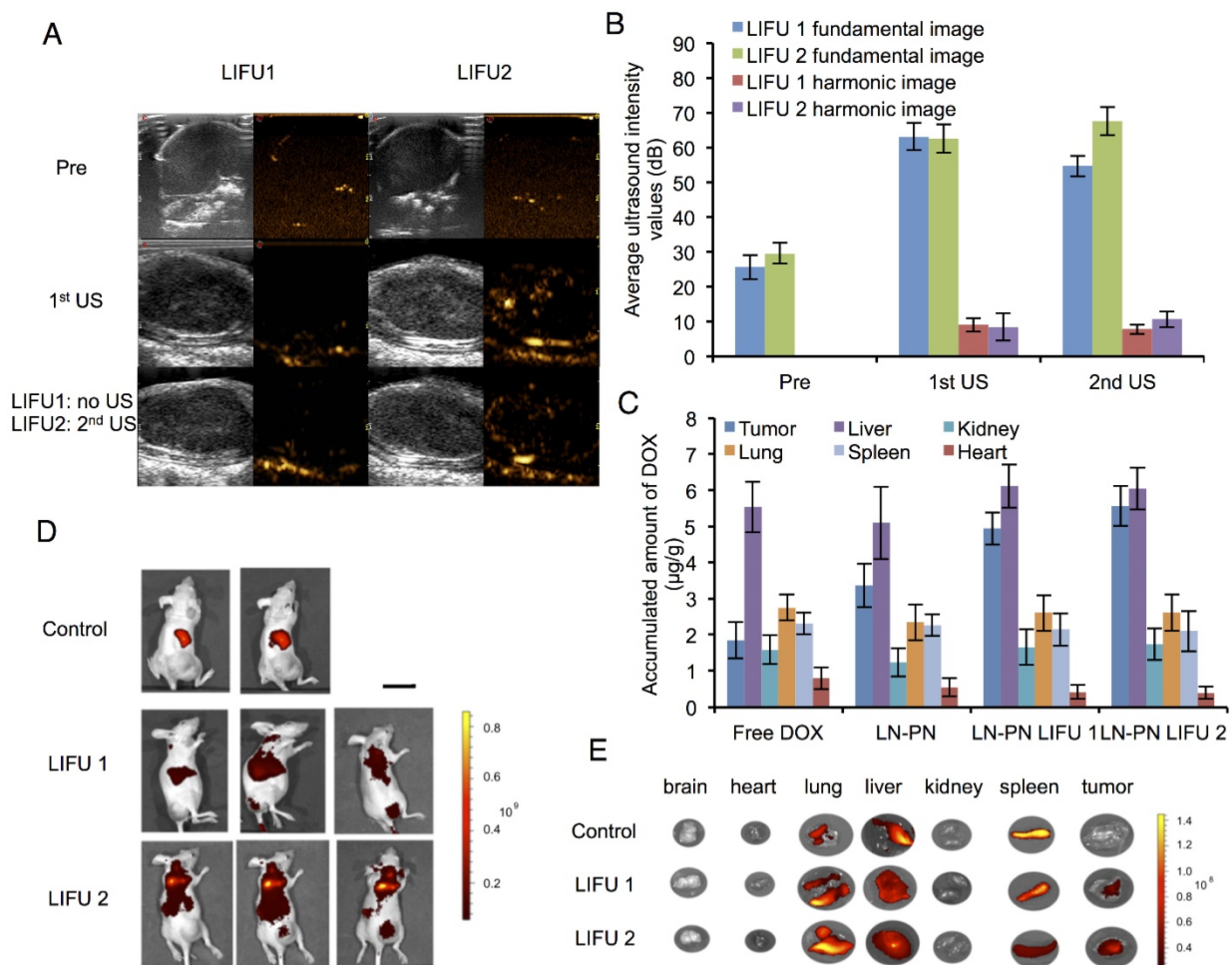
Figure 4. Ultrasound images (A) and average ultrasound intensity values (B) in tumors. Scale bar=0.3 cm. (C) *in vivo* distribution of accumulated DOX per gram tissue after intravenous injection of different formulations for 24 h. Distribution of nanodroplets labeled by DiR *in vivo* (D) and in different organs (E) (Control: no ultrasound radiation; 1: before ultrasound exposure; 2: the1st treatment; 3: the 2nd treatment) Scale bar=2.5 cm.
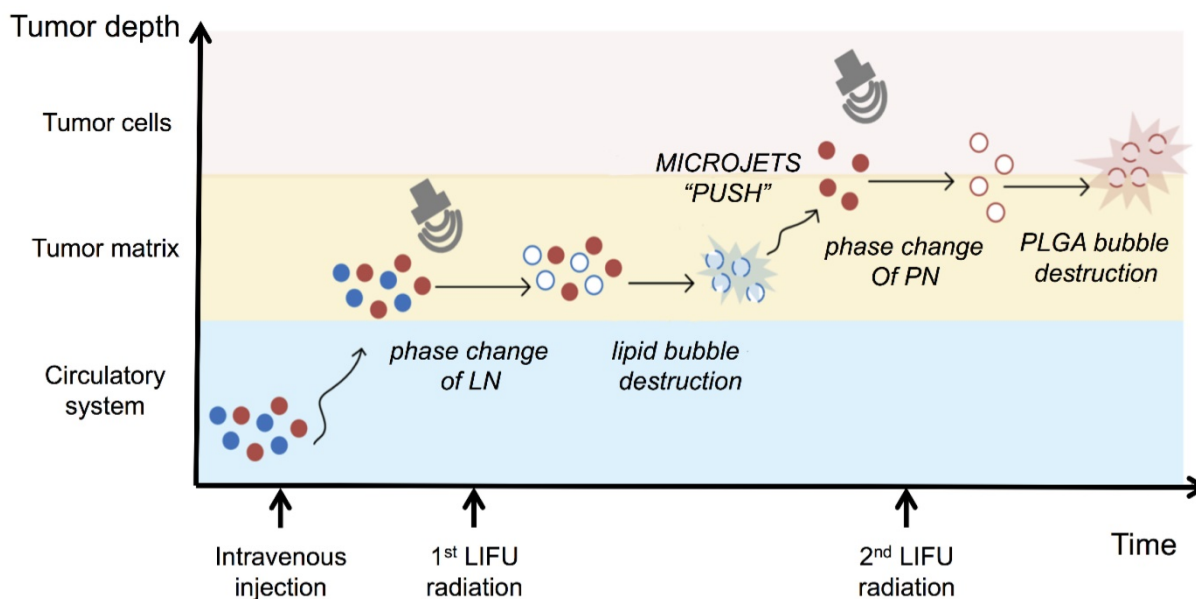

Figure 5. Schematic diagram of the release of nanodroplets complex triggered by LIFU radiation at different stages.
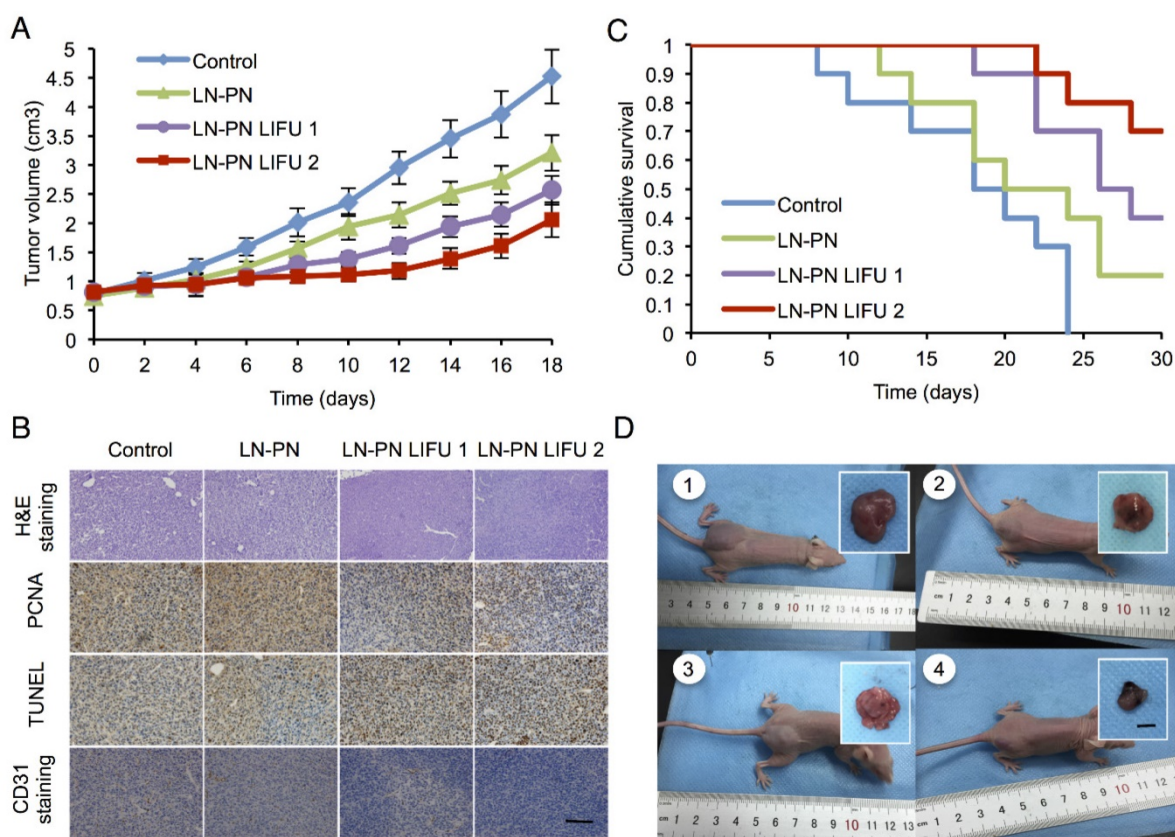
Figure 6. A) Tumor-volume curves after the injection of LN-PN followed by LIFU treatment *in vivo*; B) Cumulative survival of animals after intravenous administration of various formulations and LIFU irradiations; C) Histological characteristics of the MDA-MB 231 tumor tissues in different therapeutic groups evaluated by H&E staining, PCNA, TUNEL and CD31 staining. (×400) Scale bar=10 μm; D) Typical photographs of tumor-bearing nude mice and excised tumors from mice at the end of treatment (1: Control; 2: LN-PN; 3: LN-PN LIFU1; 4: LN-PN LIFU2) Scale bar=10 mm.

We also monitored the animal survival after intravenous administration of various formulations (Fig. 6B). Approximately 70% animals of the LIFU2 groups and 40% animals of the LIFU1 groups survived after 30 days. Only 20% animals were alive for the LN-PN group without LIFU radiation. However, all animals in the control groups died within 22 days. These data were consistent with the results of tumor-growth inhibition. The application of external LIFU enhanced the accumulation and intratumoral distribution of the drug inhibiting tumor proliferation.

The histological characteristics of breast tumor tissues after different treatments were evaluated by H&E staining, PCNA, TUNEL and CD31 staining (Fig. 6C). Compared to the LIFU-treated groups, the tumors in control LN-PN groups were hypercellular and showed higher levels of chromatin content and nuclear polymorphism as measured by H&E staining. In the LN-PN LIFU2 group, necrosis was observed in the tumor sections resulting from the therapeutic agents released from the nanodroplets under ultrasound radiation. PCNA expression manifested as brown granules in cell nuclei was observed as well. Similar to the proliferation assay,

the results of TUNEL assay displayed the same trends of cell apoptosis in different groups. We also measured microvascular density in tumor sections by CD31 staining. The expression of CD31 in the groups treated with LN-PN exposed to LIFU2 was the lowest among all four groups. CD31 expression was decreased in the LN-PN group exposed to ultrasound compared with the groups without ultrasound exposure. The microvessel density of ultrasound-triggered groups was also reduced. The combination of microbubble and low-intensity ultrasound had been investigated in the anti-vascular therapy [40, 60-62]; microbubbles-mediated acoustic energy was delivered at sites contiguous with the endothelial cells lining the neovasculature, resulting in their disruption. Multiple mechanisms were involved in this process. For example, both thermal and cavitation effects were likely to play roles varying by sonication conditions. It is likely that in the present study, microshear associated with bubble oscillation and continuous sonication resulted in the destruction of the microvasculature leading to increased drug delivery and enhanced therapeutic efficacy in tumor chemotherapy.

Conclusions

In this study, we report, for the first time, the construction of a phase-changeable drug-delivery nanosystem with the programmable LIFU-triggered drug-releasing ability for significantly enhanced anticancer drug delivery. Two types of nanodroplets were fabricated for both *in vitro* and *in vivo* evaluation. The chemotherapeutic drug DOX and ultrasound-responsive PFP were concurrently loaded into the nanodroplets for programmable drug release triggered by LIFU. Ultrasound irradiation was conducted to trigger the on-demand release of encapsulated agents from the drug carriers. Importantly, the nanodroplets could change to microbubbles when exposed to LIFU ensuring the precise and direct targeting of the ultrasound energy to the tumor sites. Based on the acoustic properties of shell materials, such as shell stiffness, various ultrasound energies were introduced to induce the phase transition and microbubble collapse of nanodroplets *in vitro* (3 W/3 min for lipid nanodroplets; 8 W/3 min for PLGA nanodroplets). Three steps were involved in the drug-releasing profiles. A sharp increase curve was realized when LIFU was irradiated. Consequently, intratumoral accumulation and distribution of the drug with LIFU2 exposure were significantly enhanced and tumor proliferation was substantially inhibited. Co-delivery of two drug-loaded nanodroplets could overcome the physical barriers of tumor tissues during chemotherapy. We believe that our work of the elaborate design of nanocarriers with specific triggering by LIFU, paves a new way for the on-demand programmable drug release and more efficient chemotherapy.

Abbreviations

LIFU: low-intensity focused ultrasound; DOX: doxorubicin; PFC: perfluoropentane; PFP: perfluorocarbon; ADV: acoustic droplet vaporization; UTMD: ultrasound targeted microbubble destruction; HIFU: high-intensity focused ultrasound; PLGA: poly(lactide-co-glycolide) acid; DPPC: dipalmitoyl phosphatidylcholine; DPPG: dipalmitoyl phospha-tidylglycerole; DPPE: dipalmitoylphosphatidyleth-anolamine; PEG: polyethyleneglycol; DMEM: high glucose dulbecco's modified eagle medium; FBS: fetal bovine serum; DiO: 3,3'-dioctadecyloxacarbocyanine perchlorate; DiR: 1,1'-dioctadecyl-3,3,3',3'-tetramethyl indotricarbocyanine iodide; EDTA: ethylenediaminet-etraacetic acid. DAPI: 4',6-diamidino-2-phenylindole; H&E: hematoxylin /eosin; PCNA: proliferating cell nuclear antigen; MVD: microvessel density; TUNEL: TdT-dependent dUTP-biotin nick end labeling. DLS: dynamic light scattering; TEM: transmission electron microscopy; EE: encapsulation efficiency.

Acknowledgments

Supplementary Material

Supplementary figures.
http://www.thno.org/v08p1327s1.pdf

Competing Interests

The authors have declared that no competing interest exists.

References

1. Hannah AS, Luke GP, Emelianov SY. Blinking phase-change nanocapsules enable background-free ultrasound imaging. Theranostics. 2016; 6: 1866-76.
2. Lee JY, Carugo D, Crake C, et al. Nanoparticle-loaded protein-polymer nanodroplets for improved stability and conversion efficiency in ultrasound imaging and drug delivery. Adv Mater. 2015; 27: 5484-92.
3. Yoon YI, Kwon YS, Cho HS, et al. Ultrasound-mediated gene and drug delivery using a microbubble-liposome particle system. Theranostics. 2014; 4: 1133-44.
4. Unger E, Porter T, Lindner J, et al. Cardiovascular drug delivery with ultrasound and microbubbles. Adv Drug Deliv Rev. 2014; 72: 110-26.
5. Kiessling F, Fokong S, Bzyl J, et al. Recent advances in molecular, multimodal and theranostic ultrasound imaging. Adv Drug Deliv Rev. 2014; 72: 15-27.
6. Park J, Aryal M, Vykhodtseva N, et al. Evaluation of permeability, doxorubicin delivery, and drug retention in a rat brain tumor model after ultrasound-induced blood-tumor barrier disruption. J Control Release. 2017; 250: 77-85.
7. Chen J, Ratnayaka S, Alford A, et al. Theranostic multilayer capsules for ultrasound imaging and guided drug delivery. ACS Nano. 2017; 11: 3135-46.
8. Min HS, Son S, You DG, et al. Chemical gas-generating nanoparticles for tumor-targeted ultrasound imaging and ultrasound-triggered drug delivery. Biomaterials. 2016; 108: 57-70.
9. Jablonowski LJ, Alfego D, Andorko JI, et al. Balancing stealth and echogenic properties in an ultrasound contrast agent with drug delivery potential. Biomaterials. 2016; 103: 197-206.
10. Fan CH, Cheng YH, Ting CY, et al. Ultrasound/magnetic targeting with SPIO-DOX-microbubble complex for image-guided drug delivery in brain tumors. Theranostics. 2016; 6: 1542-56.
11. Ektate K, Kapoor A, Maples D, et al. Motion compensated ultrasound imaging allows thermometry and image guided drug delivery monitoring from echogenic liposomes. Theranostics. 2016; 6: 1963-74.
12. Åslund AKO, Berg S, Hak S, Mørch Ý, Torp SH, Sandvig A, Widerøe M, Hansen R, de Lange DaviesC. Nanoparticle delivery to the brain--by focused ultrasound and self-assembled nanoparticle-stabilized microbubbles. J Control Release. 2015;220(Pt A): 287-94.
13. Staruch R, Chopra R, Hynynen K. Hyperthermia in bone generated with MR imaging-controlled focused ultrasound: control strategies and drug delivery. Radiology. 2012; 263: 117-27.
14. Lee S, Han H, Koo H, et al. Extracellular matrix remodeling in vivo for enhancing tumor-targeting efficiency of nanoparticle drug carriers using the pulsed high intensity focused ultrasound. J Control Release. 2017; 263: 68-78.
15. Rapoport NY, Kennedy AM, Shea JE, et al. Controlled and targeted tumor chemotherapy by ultrasound-activated nanoemulsions/microbubbles. J Control Release. 2009; 138: 268-76.
16. Wang TY, Choe JW, Pu K, et al. Ultrasound-guided delivery of microRNA loaded nanoparticles into cancer. J Control Release. 2015; 203: 99-108.
17. Gao ZG, Fain HD, Rapoport N. Controlled and targeted tumor chemotherapy by micellar-encapsulated drug and ultrasound. J Control Release. 2005; 102: 203-22.

18. Rapoport N, Gao Z, Kennedy A. Multifunctional nanoparticles for combining ultrasonic tumor imaging and targeted chemotherapy. J Natl Cancer Inst. 2007; 99: 1095-106.

19. Luo W, Wen G, Yang L, et al. Dual-targeted and pH-sensitive doxorubicin prodrug-microbubble complex with ultrasound for tumor treatment. Theranostics. 2017; 7: 452-65.

20. Keum DH, Mun JH, Hwang BW, et al. Smart microbubble eluting theranostic stent for noninvasive ultrasound imaging and prevention of restenosis. Small. 2017; 13: 1602925.

21. Xing L, Shi Q, Zheng K, et al. Ultrasound-mediated microbubble destruction (UMMD) facilitates the delivery of CA19-9 targeted and paclitaxel loaded mPEG-PLGA-PLL nanoparticles in pancreatic cancer. Theranostics. 2016; 6: 1573-87.

22. Chertok B, Langer R, Anderson DG. Spatial control of gene expression by nanocarriers using heparin masking and ultrasound-targeted microbubble destruction. ACS Nano. 2016; 10: 7267-78.

23. Tran BC, Seo J, Hall TL, Fowlkes JB, Cain CA. Microbubble-enhanced cavitation for noninvasive ultrasound surgery. IEEE Trans Ultrason Ferroelectr Freq Control. 2003;50(10): 1296-304.

24. Wilson K, Homan K, Emelianov S. Biomedical photoacoustics beyond thermal expansion using triggered nanodroplet vaporization for contrast-enhanced imaging. Nat Comm. 2012; 3: 618.

25. Couture O, Cherin E, Foster FS. Model for the ultrasound reflection from micro-beads and cells distributed in layers on a uniform surface. Phys Med Biol. 2007;15: 4189-204.

26. Kang ST, Yeh CK. Intracellular acoustic droplet vaporization in a single peritoneal macrophage for drug delivery applications. Langmuir. 2011; 27: 13183-8.

27. Mercado KP, Radhakrishnan K, Stewart K, et al. Size-isolation of ultrasound-mediated phase change perfluorocarbon droplets using differential centrifugation. J Acoust Soc Am. 2016; 139: EL142–EL148.

28. Arena CB, Novell A, Sheeran PS, et al. Dual-frequency acoustic droplet vaporization detection for medical imaging. IEEE Trans Ultrason Ferroelectr Freq Control. 2015; 62: 1623-33.

29. Ho YJ, Chang YC, Yeh CK. Improving nanoparticle penetration in tumors by vascular disruption with acoustic droplet vaporization. Theranostics. 2016; 6: 392-403.

30. Juliar BA, Bromley MM, Moncion A, et al. In situ transfection by controlled release of lipoplexes using acoustic droplet vaporization. Adv Healthc Mater. 2016; 5: 1764-74.

31. Chen S, Grayburn PA. Ultrasound-targeted microbubble destruction for cardiac gene delivery. Methods Mol Biol. 2017; 1521: 205-18.

32. Zhao YZ, Zhang M, Wong HL, et al. Prevent diabetic cardiomyopathy in diabetic rats by combined therapy of aFGF-loaded nanoparticles and ultrasound-targeted microbubble destruction technique. J Control Release. 2016; 223: 11-21.

33. Lo AH, Kripfgans OD, Carson PL, Rothman ED, Fowlkes JB. Acoustic droplet vaporization threshold: effects of pulse duration and contrast agent. IEEE Trans Ultrason Ferroelectr Freq Control. 2007;54(5): 933-46.

34. Tinkov S, Coester C, Serba S, et al. New doxorubicin-loaded phospholipid microbubbles for targeted tumor therapy: in-vivo characterization. J Control Release. 2010; 148: 368-72.

35. Muthupillai R, Lomas DJ, Rossman PJ, et al. Magnetic resonance elastography by direct visualization of propagating acoustic strain waves. Science. 1995; 269: 1854-7.

36. Tinkov S, Bekeredjian R, Winter G, et al. Microbubbles as ultrasound triggered drug carriers. J Pharm Sci. 2009; 98: 1935-61.

37. Wu SY, Chen CC, Tung YS, et al. Effects of the microbubble shell physicochemical properties on ultrasound-mediated drug delivery to the brain. J Control Release. 2015; 212: 30-40.

38. Borden MA, Kruse DE, Caskey CF, et al. Influence of lipid shell physicochemical properties on ultrasound-induced microbubble destruction. IEEE Trans Ultrason Ferroelectr Freq Control. 2005; 52: 1992-2002.

39. Yin T, Wang P, Li J, et al. Tumor-penetrating codelivery of siRNA and paclitaxel with ultrasound-responsive nanobubbles hetero-assembled from polymeric micelles and liposomes. Biomaterials. 2014; 35: 5932-43.

40. Wood AK, Sehgal CM. A review of low-intensity ultrasound for cancer therapy. Ultrasound Med Biol. 2015; 41: 905-28.

41. Reznik N, Lajoinie G, Shpak O, et al. On the acoustic properties of vaporized submicron perfluorocarbon droplets. Ultrasound Med Biol. 2014; 40: 1379-84.

42. Reznik N, Shpak O, Gelderblom EC, et al. The efficiency and stability of bubble formation by acoustic vaporization of submicron perfluorocarbon droplets. Ultrasonics. 2013; 53: 1368-76.

43. Chaussy CG, Thuroff S. High-intensity focused ultrasound for the treatment of prostate cancer: A review. J Endourol. 2017; 31: S30-S37.

44. Lang BH, Woo YC, Wong CKH. High-intensity focused ultrasound for treatment of symptomatic benign thyroid nodules: a prospective study. Radiology. 2017; 18: 161640.

45. Zhou YF. High intensity focused ultrasound in clinical tumor ablation. World J Clin Oncol. 2011; 2: 8-27.

46. Liu J, Shang T, Wang F, et al. Low-intensity focused ultrasound (LIFU)-induced acoustic droplet vaporization in phase-transition perfluoropentane nanodroplets modified by folate for ultrasound molecular imaging. Int J Nanomedicine. 2017; 12: 911-23.

47. Rezayat E, Toostani IG. A review on brain stimulation using low intensity focused ultrasound. Basic Clin Neurosci. 2016; 7: 187-94.

48. Rizzitelli S, Giustetto P, Cutrin JC, et al. Sonosensitive theranostic liposomes for preclinical in vivo MRI-guided visualization of doxorubicin release stimulated by pulsed low intensity non-focused ultrasound. J Control Release. 2015; 202: 21-30.

49. Iyer AK, Khaled G, Fang J, et al. Exploiting the enhanced permeability and retention effect for tumor targeting. Drug Disc Today. 2006; 11: 812-8.

50. Hobbs SK, Monsky WL, Yuan F, et al. Regulation of transport pathways in tumor vessels: role of tumor type and microenvironment. Proc Natl Acad Sci USA. 1998; 95: 4607-12.

51. Perry JL, Reuter KG, Luft JC, et al. Mediating passive tumor accumulation through particle size, tumor type, and location. Nano Lett. 2017; 17: 2879-86.

52. Sykes EA, Chen J, Zheng G, et al. Investigating the impact of nanoparticle size on active and passive tumor targeting efficiency. ACS Nano. 2014; 8: 5696-706.

53. Nomikou N, McHale AP. Exploiting ultrasound-mediated effects in delivering targeted, site-specific cancer therapy. Cancer Lett. 2010; 296: 133-43.

54. Liu HL, Fan CH, Ting CY, et al. Combining microbubbles and ultrasound for drug delivery to brain tumors: current progress and overview. Theranostics. 2014; 4: 432-44.

55. Fan CH, Lin WH, Ting CY, et al. Contrast-enhanced ultrasound imaging for the detection of focused ultrasound-induced blood-brain barrier opening. Theranostics. 2014; 4: 1014-25.

56. Chen CC, Sheeran PS, Wu SY, et al. Targeted drug delivery with focused ultrasound-induced blood-brain barrier opening using acoustically-activated nanodroplets. J Control Release. 2013; 172: 795-804.

57. Song KH, Fan AC, Hinkle JJ, et al. Microbubble gas volume: A unifying dose parameter in blood-brain barrier opening by focused ultrasound. Theranostics. 2017; 7: 144-52.

58. Huang Y, Alkins R, Schwartz ML, et al. Opening the blood-brain barrier with MR imaging-guided focused ultrasound: preclinical testing on a trans-human skull porcine model. Radiology. 2017; 282: 123-30.

59. Huang HY, Liu HL, Hsu PH, et al. A multitheragnostic nanobubble system to induce blood-brain barrier disruption with magnetically guided focused ultrasound. Adv Mater. 2015; 27: 655-61.

60. Lin CY, Li JR, Tseng HC, et al. Enhancement of focused ultrasound with microbubbles on the treatments of anticancer nanodrug in mouse tumors. Nanomedicine. 2012; 8: 900-7.

61. Hu B, Cai XZ, Shi ZL, et al. Microbubble injection enhances inhibition of low-intensity pulsed ultrasound on debris-induced periprosthetic osteolysis in rabbit model. Ultrasound Med Biol. 2015; 41: 177-86.

62. Zhao X, Li L, Zhao H, et al. Liver haemostasis using microbubble-enhanced ultrasound at a low acoustic intensity. Eur Radiol. 2012; 22: 379-86.